

## 2D Materials



### PAPER

# Atomically resolved FeSe/SrTiO<sub>3</sub>(001) interface structure by scanning transmission electron microscopy

RECEIVED  
16 December 2015

REVISED  
6 February 2016

ACCEPTED FOR PUBLICATION  
22 February 2016

PUBLISHED  
30 March 2016

Fangsen Li<sup>1,6</sup>, Qinghua Zhang<sup>2,6</sup>, Chenjia Tang<sup>1</sup>, Chong Liu<sup>1</sup>, Jinan Shi<sup>3</sup>, CaiNa Nie<sup>1</sup>, Guanyu Zhou<sup>1</sup>, Zheng Li<sup>1</sup>, Wenhao Zhang<sup>1</sup>, Can-Li Song<sup>1,4</sup>, Ke He<sup>1,4</sup>, Shuaihua Ji<sup>1,4</sup>, Shengbai Zhang<sup>5</sup>, Lin Gu<sup>3,4</sup>, Lili Wang<sup>1,4</sup>, Xu-Cun Ma<sup>1,4</sup> and Qi-Kun Xue<sup>1,4</sup>

<sup>1</sup> State Key Laboratory of Low-Dimensional Quantum Physics, Department of Physics, Tsinghua University, Beijing 100084, People's Republic of China

<sup>2</sup> State Key Laboratory of New Ceramics and Fine Processing, School of Materials Science and Engineering, Tsinghua University, Beijing 100084, People's Republic of China

<sup>3</sup> Institute of Physics, Chinese Academy of Science, Beijing 100190, People's Republic of China

<sup>4</sup> Collaborative Innovation Center of Quantum Matter, Beijing 100084, People's Republic of China

<sup>5</sup> Department of Physics, Applied Physics and Astronomy, Rensselaer Polytechnic Institute, Troy, NY 12180, USA

<sup>6</sup> These authors contributed equally to this work.

E-mail: [l.gu@iphy.ac.cn](mailto:l.gu@iphy.ac.cn) and [liliwang@mail.tsinghua.edu.cn](mailto:liliwang@mail.tsinghua.edu.cn)

Keywords: FeSe films, SrTiO<sub>3</sub>, interface superconductivity, interface structure

### Abstract

Interface-enhanced high-temperature superconductivity in one unit-cell FeSe films on SrTiO<sub>3</sub>(001) (STO) substrate has recently attracted much attention in condensed matter physics and material science. By combined *in situ* scanning tunneling microscopy/spectroscopy and *ex situ* scanning transmission electron microscopy studies, we report on atomically resolved structure including both lattice constants and actual atomic positions of the FeSe/STO interface under both non-superconducting and superconducting states. We observed TiO<sub>2</sub> double layers and significant atomic displacements in the top two layers of STO, lattice compression of the Se–Fe–Se triple layer, and relative shift between bottom Se and topmost Ti atoms. By imaging the interface structures under various superconducting states, we unveil a close correlation between interface structure and superconductivity. Our atomic-scale identification of FeSe/STO interface structure provides insight on investigating the pairing mechanism of this interface-enhanced high-temperature superconducting system.

### Introduction

The discovery of a superconducting gap  $\Delta \sim 20$  meV, nearly one order of magnitude higher than that of bulk FeSe, in one unit-cell (UC) FeSe film grown on SrTiO<sub>3</sub>(001) (STO) substrate [1] has stimulated much attention in superconductivity community. The superconducting transition temperatures ( $T_c$ ) ranging from 50 K to 100 K were subsequently revealed by transport [2–5] and mutual inductance measurements [2, 6]. Compared with  $T_c \sim 9$  K for bulk FeSe [7], the above findings indicate a vital role of STO substrate in boosting the high temperature superconductivity. Previous angle-resolved photoemission spectroscopy (ARPES) [8–11] and scanning tunneling microscopy/spectroscopy (STM/STS) studies [12] have revealed significant charge transfer from STO substrate to FeSe

films, which can be controlled by vacuum annealing [9, 12]. It is widely believed that the electrons injected into FeSe films originate from oxygen vacancies in STO [10, 12–14]. However, atomic structure of the interface and how the doping is realized with annealing are still elusive. In addition to interface charge transfer, coupling between FeSe electrons and high-energy optical phonons in STO is suggested by ARPES study as occurrence of a replica band separated by  $\sim 100$  meV from the main band [15]. In terms of the energy of  $\sim 100$  meV, the responsible phonon should be a polar phonon mode on the surface layer of the STO substrate that is related to Ti–O displacement near surface [15–18]. Very recently, features of electron–phonon coupling with two low energy phonon modes at  $\sim 11$  meV and  $\sim 21$  meV, are observed in STS studies [19], in good agreement with the first-principle

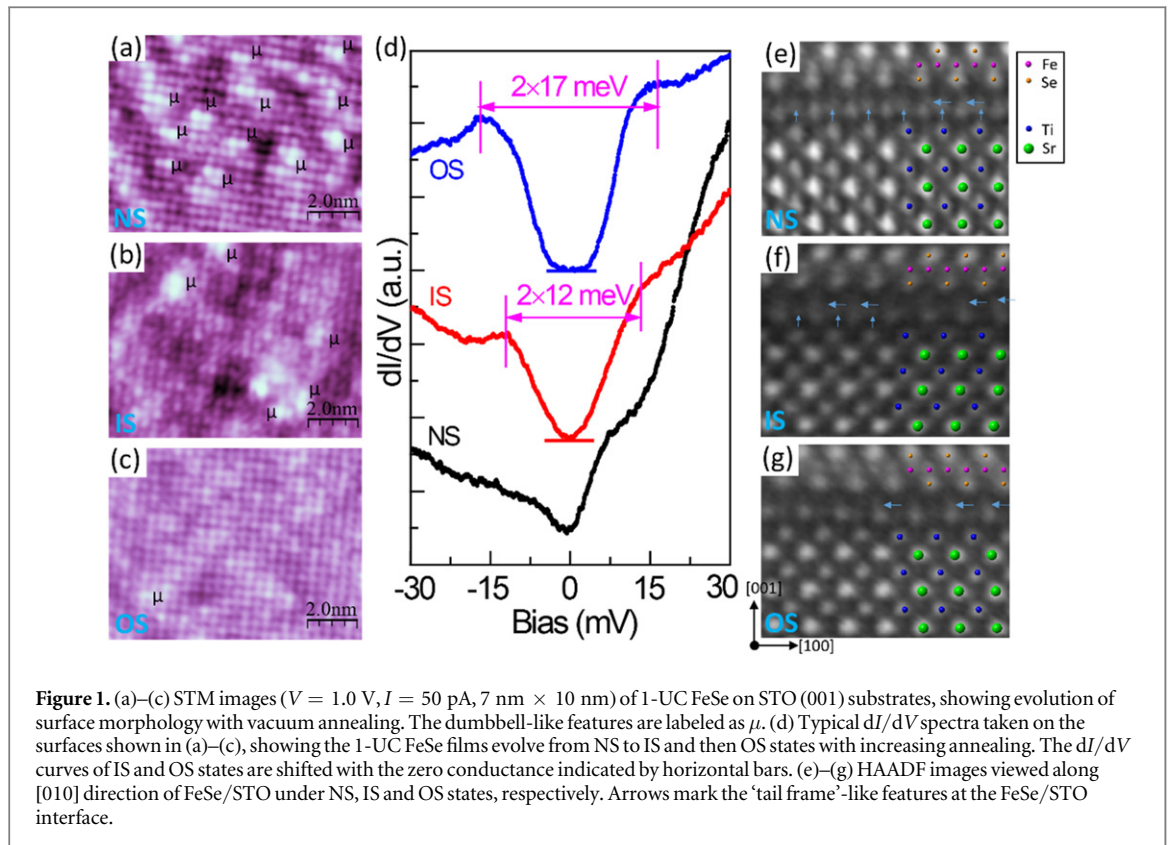


**Figure 1.** (a)–(c) STM images ( $V = 1.0$  V,  $I = 50$  pA,  $7$  nm  $\times$   $10$  nm) of 1-UC FeSe on STO (001) substrates, showing evolution of surface morphology with vacuum annealing. The dumbbell-like features are labeled as  $\mu$ . (d) Typical  $dI/dV$  spectra taken on the surfaces shown in (a)–(c), showing the 1-UC FeSe films evolve from NS to IS and then OS states with increasing annealing. The  $dI/dV$  curves of IS and OS states are shifted with the zero conductance indicated by horizontal bars. (e)–(g) HAADF images viewed along [010] direction of FeSe/STO under NS, IS and OS states, respectively. Arrows mark the 'tail frame'-like features at the FeSe/STO interface.

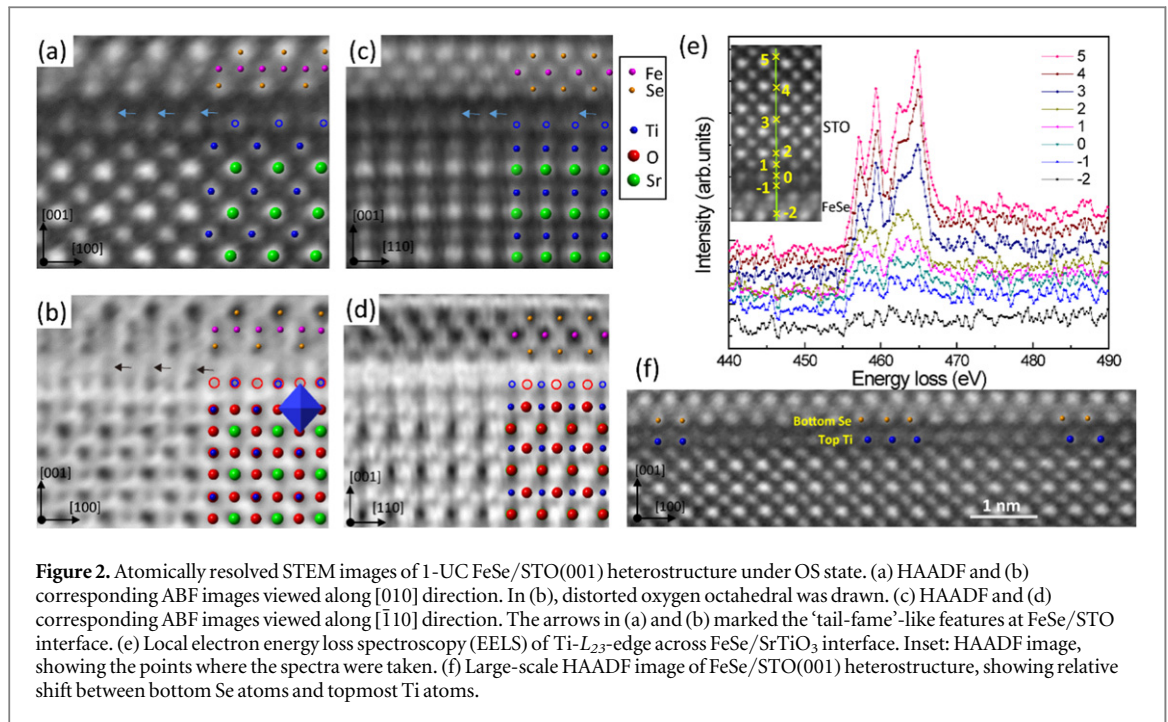
calculation that takes the template effect of STO substrate into account [20]. To understand these phenomena and superconductivity mechanism, atomic-scale information on the FeSe/STO interface is indispensable. In this study, we combine high-resolution scanning transmission electron microscopy (STEM) and STM/STS to investigate both in-plane and out-of-plane atomic structure of the interface. By studying the interface structures under both non-superconducting and superconducting samples, we reveal a close relation between interface structure and superconducting properties.

## Results and discussion

Figure 1 shows the evolution of surface morphology, corresponding tunneling spectra and interface structure of 1-UC FeSe films on STO with ultra-high vacuum (UHV) annealing. The atomically resolved STM images (figures 1(a)–(c)) all display Se-terminated (001) FeSe surface with an in-plane lattice constant of  $\sim 3.9$  Å, which is the same as that of STO(001) surface and thus 3% larger than the value of 3.77 Å for bulk FeSe [7]. Dumbbell-like features (labeled as  $\mu$ ) are observed in figures 1(a) and (b), which correspond to extra Se atoms in Se–Fe–Se triple layers under the Se-rich growth condition [21]. When the extra Se atoms desorb with annealing, the 1-UC FeSe films convert from non-superconducting (NS) (black curve in figure 1(d)) to superconducting states with a gap of 12 meV and 17 meV (red

and blue curves in figure 1(d), respectively). To simplify the description, we named the three different states as NS, intermediate superconducting (IS), and optimal superconducting (OS) states, respectively.

Displayed in figure 2 are detailed STEM results of the FeSe/STO interface in OS state. Figures 2(a) and (c) ((b) and (d)) show typical atomically resolved high-angle annular dark field (HAADF) (annular bright-field (ABF)) images viewed along the [010] and  $[\bar{1}10]$  directions, respectively. In the HAADF images, Se, Fe, Sr and Ti atoms appear as bright dots and are clearly identified with sharp intensity contrast, while in the ABF images those atoms appear as dark dots and O atoms bright. An ordered Se–Fe–Se triple layer is clearly observed, except that top layer Se atoms look brighter than the bottom layer Se atoms, indicative of substitution of Te for Se [22]. Nevertheless, *ex situ* transport studies after capping FeTe layer demonstrate systematically increasing  $T_c$  with annealing [12], attesting to the three distinct states for STEM measurement. On the STO side,  $\text{TiO}_2$  and SrO layers stack in sequence. Intriguingly, an extra layer, marked by blue circles in figures 2(a)–(d), is noticed right below the bottom Se layer. The atom columns in this extra layer is located nearly at the positions of Sr columns, but exhibit intensity similar to Ti columns. With O atoms in this extra layer disclosed in the corresponding ABF images, marked by red circles in figures 2(b) and (d), we infer the extra layer as  $\text{TiO}_x$  layer based on previous studies [23–27].



To identify the chemical composition of the extra layer, we conducted atomically resolved electron energy loss spectroscopy (EELS) of Ti- $L_{23}$  edge across the FeSe/STO interface. The results are shown in figure 2(e). At points far away from the interface, such as point ‘5’, the spectrum shows four peaks in an energy range of 455–470 eV, similar to the typical characteristic of Ti- $L_{23}$ -edge observed in bulk STO with oxygen vacancy concentration  $\delta < 0.13$  (SrTiO<sub>3- $\delta$ ) reported previously [28], indicative of near Ti<sup>4+</sup>. The oxygen vacancies in STO bulk could be induced during the high temperature UHV annealing [10]. Approaching to the interface, the four characteristic peaks decrease successively in intensity and merge into two wide humps (points 2, 1, 0 and –1), indicating that partial Ti<sup>4+</sup> atoms change to Ti<sup>3+</sup> as resulted from the significantly increased oxygen vacancies [28] near the surface of STO. The features of Ti<sup>3+</sup> are clearly discerned at point ‘0’ and ‘–1’ just below the Se layer, explicitly demonstrating that the extra layer is TiO<sub>x</sub> layer. Thus, a TiO<sub>x</sub> double layers (DLs) at the FeSe/STO interface is identified. The fact that this TiO<sub>x</sub> DLs occurs at the FeSe/STO interface irrespective of NS, IS or OS states (figures 1(e)–(g)), together with the TiO<sub>x</sub> rich surface of STO(001) reported previously [23–27], indicates that the TiO<sub>x</sub> DLs is intrinsic characteristic of STO(001). Compared with previous STEM results [25], the TiO<sub>x</sub> DLs is much more clearly resolved because of the sharp interface between single crystalline FeSe films and STO. To distinguish the two TiO<sub>x</sub> layers, we name the extra TiO<sub>x</sub> layer as top TiO<sub>x</sub> layer, and the other as the 1st TiO<sub>x</sub> layer of bulk STO.</sub>

A closer examination of the TiO<sub>x</sub> DLs reveals some ‘tail frame’-like features with weak contrast around Ti columns, as indicated by arrows in figures 1(e)–(g) and

2(a)–(c). Statistics on more than ten different regions of each sample shows that the ‘tail frame’-like features decrease gradually in both density and weight from NS to IS and then OS state, which is also evidenced from the HAADF images shown in figures 1(e)–(g). Considering the corresponding surface morphology evolution, i.e. desorption of extra Se atoms in Se–Fe–Se triple layers with annealing, seen from the STM topography images shown in figures 1(a)–(c), we speculate that the ‘tail frame’-like features correspond to extra Se atoms at the FeSe/STO interface, which may incorporate into the top TiO<sub>x</sub> layer and compensate some oxygen vacancies on STO surface.

To bring more insight into the correlation between structure and superconductivity properties, we quantified the interface structure by measuring various inter-atomic distances at NS, IS and OS states depicted in the schematic model in figure 3(a). It is worthy to note that to reduce the error induced by Te/Se mixing, the Se height  $h_{\text{Se}}$  here is measured as the distance between iron layer and bottom Se layer. The results are summarized in figure 3(b) and table 1. As displayed in figure 3(b), the distance between the double TiO<sub>x</sub> layers is  $2.44 \text{ \AA} \pm 0.08 \text{ \AA}$ , which is  $\sim 25\%$  larger than half of the lattice constant of STO along the [001] direction and independent of the sample states. Both the 1st TiO<sub>x</sub> and 1st SrO layer shrink inwards, as evidenced from the reduced nearest neighboring (NN) layer distance of  $1.81 \text{ \AA} \pm 0.05 \text{ \AA}$  and  $1.85 \text{ \AA} \pm 0.09 \text{ \AA}$ , respectively. For the 2nd TiO<sub>2</sub> and deeper layers, the atomic displacements are negligible. Consistent with the in-plane lattice of  $\sim 3.9 \text{ \AA}$  revealed by STM, identical in-plane lattice constant (the Se–Se distance,  $a_{\text{FeSe}}$ ) of  $\sim 3.86 \text{ \AA}$  is observed in the FeSe films under the three distinct states. Intriguingly, when the film changes

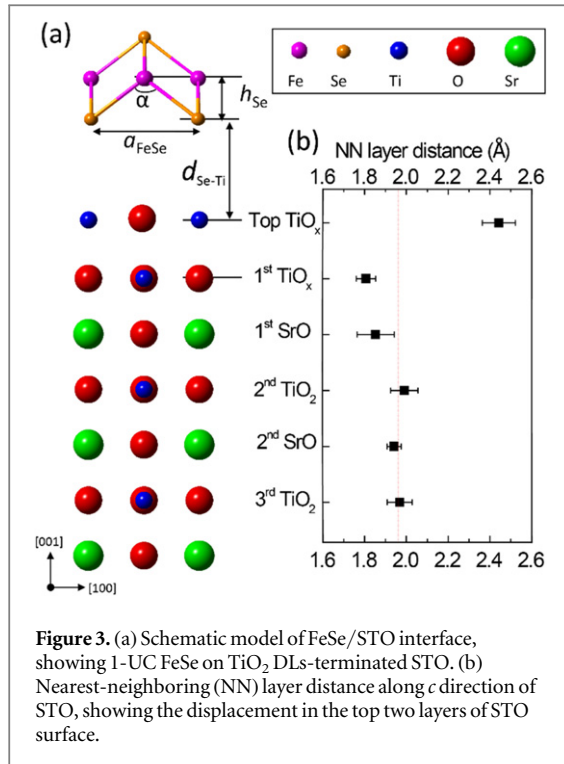


**Figure 3.** (a) Schematic model of FeSe/STO interface, showing 1-UC FeSe on  $\text{TiO}_2$  DLs-terminated STO. (b) Nearest-neighboring (NN) layer distance along  $c$  direction of STO, showing the displacement in the top two layers of STO surface.

**Table 1.** Structure parameters of FeSe/SrTiO<sub>3</sub> interface under various superconducting states (NS, IS and OS): lattice constant  $a_{\text{FeSe}}$ , anion height  $h_{\text{Se}}$ , angle  $\alpha$  of Se–Fe–Se bonding, and distance  $d_{\text{Se-Ti}}$  between bottom Se and topmost Ti atoms.

	NS	IS	OS
$a_{\text{FeSe}}/\text{Å}$	$3.87 \pm 0.02$	$3.85 \pm 0.02$	$3.86 \pm 0.03$
$h_{\text{Se}}/\text{Å}$	$1.33 \pm 0.02$	$1.32 \pm 0.02$	$1.31 \pm 0.01$
$\alpha$	$111.0^\circ \pm 0.9^\circ$	$111.0^\circ \pm 0.7^\circ$	$111.4^\circ \pm 0.9^\circ$
$d_{\text{Se-Ti}}/\text{Å}$	$3.34 \pm 0.05$	$3.47 \pm 0.07$	$3.58 \pm 0.05$

from NS to OS state, the Se height  $h_{\text{Se}}$  decreases from  $1.33 \text{ Å} \pm 0.02 \text{ Å}$  to  $1.31 \text{ Å} \pm 0.01 \text{ Å}$ , whereas the separation  $d_{\text{Se-Ti}}$  between the bottom Se layer and the topmost Ti layer increases from  $3.34 \text{ Å} \pm 0.05 \text{ Å}$  to  $3.58 \text{ Å} \pm 0.05 \text{ Å}$  (table 1).

We now focus on the interface structure of the OS sample. The Se–Se distance is  $3.86 \text{ Å} \pm 0.03 \text{ Å}$ ,  $\sim 2.4\%$  expanded compared to the value of  $3.77 \text{ Å}$  for bulk FeSe [7] and close to the in-plane lattice constant of STO substrate ( $3.9 \text{ Å}$ ). As demonstrated by previous STM studies, 1-UC FeSe films on STO consist of high density of domains [29, 30], and exhibit  $2 \times 1$  reconstruction [1] and strong atomic distortion within each domain [19]. Consistent with the finding that  $2 \times 1$  reconstruction in 1-UC FeSe films is purely an electronic feature instead of lattice reconstruction as revealed by AFM study [31], no such reconstruction is observed in STEM images. Whereas, the random atomic distortion [19] originates from structure, as relative shift between the bottom Se atoms and the topmost Ti atoms along the in-plane direction is clearly discerned from the STEM images shown in figure 2(f). Since the relative shift is always observed irrespective of dark or

bright domain walls (not shown) in FeSe films, on which FeSe films are separated with a constant width of  $1.5a_{\text{Se-Se}}$  [29] and continuous [30], respectively, we exclude its relation to domain walls. To compensate the in-plane expansion, the Se height  $h_{\text{Se}}$  reduces to  $1.31 \text{ Å} \pm 0.01 \text{ Å}$ ,  $\sim 9.5\%$  lower than that of bulk FeSe ( $1.45 \text{ Å}$ ) [7]. Consequently, the Se–Fe–Se bond angle  $\alpha$  changes to  $\sim 111.4^\circ \pm 0.9^\circ$ , which is close to that of a regular tetrahedron ( $\sim 109.5^\circ$ ).

The atomic-resolved FeSe/STO interface structures shown above have several implications, which shed insight on understanding the mechanism of high temperature superconductivity in FeSe/STO system. First, it rules out the tensile stress as a key factor that induces the high temperature superconductivity in FeSe/STO. Compared to bulk FeSe, the 1-UC FeSe films on STO exhibit more two-dimensional essential Se–Fe–Se triple layer ( $\sim 9.5\%$  compressed  $h_{\text{Se}}$ ) and much larger superconducting gap ( $\sim 20 \text{ meV}$ ). This seems to be consistent with the empirical rule in bulk iron chalcogenides that the superconductivity is enhanced as the Se height  $h_{\text{Se}}$  above the Fe layer is reduced [32, 33]. However, the value of  $h_{\text{Se}}$  observed here is far from the optimal value of  $1.38 \text{ Å}$  [34]. Moreover, regardless of the significant local structure distortion in 1-UC FeSe films (figure 2(f)), the superconducting gap is spatially uniform as revealed by STS studies [1, 30], consistent with the previous observations that additional  $\sim 2\%$  expansion in single-layer FeSe films [35] only induces a subtle increase of gap-closing temperature ( $T_g$ ) of 5 K and that anisotropic FeSe films on STO(110) substrates show comparable superconducting gap ( $17 \text{ meV}$ ) [36].

Second, it provides a possible picture how the interface charge transfer is achieved with annealing. In the NS state, the extra Se atoms not only exist in FeSe films (dumbbell-like features in figure 1(a)) but also incorporate in the top  $\text{TiO}_x$  layer to compensate some oxygen vacancies at FeSe/STO interface (‘tail frame’-like features in figure 1(e)). The extra Se atoms act as hole dopants for 1-UC FeSe films as revealed by first principal calculations [37, 38] and evidenced by ARPES [9] and STS studies [12], which may partially or even totally counteract the electron doping from the oxygen vacancies. Correspondingly, NS samples exhibit both hole pocket slight below Fermi level at the Brillouin zone center and electron pockets at the zone corner [9]. Once these extra Se atoms in FeSe films and at FeSe/STO interface are removed after extensive annealing, oxygen vacancies are released, promoting charge transfer from STO to FeSe. The resulted electron doping pushes the hole bands at the Brillouin zone center from the Fermi energy [9, 10, 15]. We speculate that the release of oxygen vacancies with interfacial Se desorption can activate simultaneously the interface enhanced electron–phonon coupling as proposed by two separate theoretical works [18, 39].

Third, it helps us to improve our understanding on the contribution of STO phonons to the high

temperature superconductivity. The phonon mode ( $\sim 80$ – $100$  meV) that contributes to the interface enhanced electron–phonon coupling as suggested by ARPES study [15], is claimed to correspond to a special oxygen-vacancy induced flat phonon mode which is mainly composed of relative Ti and O atomic displacements along (001) direction in the top two layers and appear exclusively at a relaxed surface [18]. The inward shrinking of the 1st TiO<sub>2</sub> and 1st SrO layer observed here (figure 3(b)) agrees qualitatively with the relaxed surface model proposed in [18]. However, the calculation in [18] is based on single TiO<sub>2</sub> terminated STO. The double TiO<sub>2</sub> termination could induce divergence in phonons from those of single TiO<sub>2</sub> terminated STO, which deserves further theoretical calculation.

At last, it challenges our understanding on the interaction between FeSe films and STO substrates. Associated with the charge transfer achieved with annealing, the separation between the bottom Se layer and the topmost Ti layer  $d_{\text{Se-Ti}}$  increases from 3.34 to 3.58 Å. These separation values are totally larger than the typical length of chemical bonds and the tendency contradicts the prediction of sink down of FeSe towards the STO substrate associated with charge transfer [13]. This finding, together with the local relative lattice shift between bottom Se atoms and topmost Ti atoms (figure 2(f)), suggests that the bonding between FeSe films and STO substrate was not such strong as expected [13]. Whether the minor increase of  $\sim 0.24$  Å in the interface separation  $d_{\text{Se-Ti}}$  from NS to OS state is crucial for boosting the high temperature superconductivity or trivial due to desorption of interfacial Se or increasing repulsion associated with charge transfer needs to be further explored.

## Conclusions

Atomically resolved STM and STEM images have been successfully achieved to reveal the atomic-scale interface structure of FeSe/STO. TiO<sub>x</sub> DLs with apparent atomic displacements are clearly identified at FeSe/STO interface. We observe a compressed Se–Fe–Se triple layer and a clear lattice shift between FeSe films and STO substrates. By studying the interface structures under different states, we unveil the correlation between interface structure and superconductivity properties. Our results demonstrate the important roles of charge transfer and interface electron–phonon coupling in the high temperature superconductivity in FeSe/STO systems.

## Materials and methods

### Growth of FeSe films on SrTiO<sub>3</sub>

One UC FeSe films were epitaxially grown on Nb-doped SrTiO<sub>3</sub>(001) (Nb: 0.5 wt%, KMT) substrates at 400 °C by co-depositing high purity Fe (99.995%) and

Se (99.9999%) in standard Knudsen cells with a flux ratio of  $\sim 1:10$ . Prior to film growth, as-received Nb:STO substrates were treated by Se molecular beam etching method [1] to achieve atomically flat surface. The superconductivity state of FeSe films was controlled by annealing time [9] and annealing temperature [12]. Here, we annealed the samples under 450 °C for 1 h, 8 h and 15 h for NS, IS and OS states, respectively. To protect FeSe films from being oxidized for *ex situ* STEM measurement, 10-UC thick FeTe films were grown by co-evaporating Fe (99.995%) and Te (99.9999%) at a substrate temperature of 300 °C.

### STM/STS characterization

STM/STS experiments were carried out in a low-temperature Createc STM system with a polycrystalline Pt/Ir tip. All the STM images and STS spectra were obtained at 4.6 K. The STS tunneling spectra were acquired using lock-in technique with a bias modulation of 3 mV at 981.3 Hz. The STM images were processed using WSxM.

### STEM characterization

STEM experiments were performed on an aberration-corrected ARM-200CF (JEOL, Tokyo, Japan) at room temperature, which was operated at 200 keV and equipped with double spherical aberration (Cs) correctors. The attainable resolution of the probe defined by the objective pre-field is 78 picometers. For each EEL spectrum, the measured step is 0.2 nm. STEM samples were prepared using focused ion beam method. Cross-sectional lamella was thinned down to 100 nm thick at an accelerating voltage of 30 kV with a decreasing current from the maximum 2.5 nA, followed by fine polish at an accelerating voltage of 2 kV with a small current of 40 pA. All STEM images were corrected for drift with the lattice constant of Sr  $\sim 3.905$  Å deep in the bulk.

To precisely measure layers' distance along *c* direction, we projected the intensity of columns in HAADF images to [001] axis along [100] direction. Peaks in the projected curve correspond to the layers' vertical positions and the distance between adjacent peaks is defined as the vertical separation between layers. We did statistics on more than ten different regions of each sample under NS, IS and OS states.

## Acknowledgments

This work is supported by Ministry of Science and Technology of China (Grants No. 2015CB921000 and No. 2014CB921002) and National Science Foundation of China (Grants No. 91421312 and No. 11574174) and the Strategic Priority Research Program of the Chinese Academy of Sciences (Grant No. XDB07030200). SBZ were supported by the US-DOE under Grant No. DESC0002623.

## References

- [1] Wang Q Y *et al* 2012 Interface-induced high-temperature superconductivity in single unit-cell FeSe films on SrTiO<sub>3</sub> *Chin. Phys. Lett.* **29** 037402
- [2] Zhang W H *et al* 2014 Direct observation of high temperature superconductivity in one-unit-cell FeSe films *Chin. Phys. Lett.* **31** 017401
- [3] Deng L Z, Lv B, Wu Z, Xue Y Y, Zhang W H, Li F S, Wang L L, Ma X-C, Xue Q-K and Chu C W 2014 Meissner and mesoscopic superconducting states in 1–4 unit-cell FeSe films *Phys. Rev. B* **90** 214513
- [4] Sun Y, Zhang W H, Xing Y, Li F S, Zhao Y F, Xia Z C, Wang L L, Ma X-C, Xue Q-K and Wang J 2014 High temperature superconducting FeSe films on SrTiO<sub>3</sub> substrates *Sci. Rep.* **4** 6040
- [5] Ge J-F, Liu Z-L, Liu C H, Gao C-L, Qian D, Xue Q-K, Liu Y and Jia J-F 2014 Superconductivity above 100 K in 1-UC FeSe films on doped SrTiO<sub>3</sub> *Nat. Mater.* **14** 285
- [6] Zhang Z C, Wang Y-H, Song Q, Liu C, Peng R, Moler K A, Feng D L and Wang Y Y 2015 Onset of the Meissner effect at 65 K in FeSe thin film grown on Nb-doped SrTiO<sub>3</sub> substrate *Sci. Bull.* **60** 1301
- [7] Hsu F C *et al* 2008 Superconductivity in the PbO-type structure  $\alpha$ -FeSe *Proc. Natl Acad. Sci. USA* **105** 14262
- [8] Liu D *et al* 2012 Electronic origin of high-temperature superconductivity in single-layer FeSe superconductor *Nat. Commun.* **3** 931
- [9] He S L *et al* 2013 Phase diagram and electronic indication of high-temperature superconductivity at 65 K in 1-UC FeSe films *Nat. Mater.* **12** 605
- [10] Tan S *et al* 2013 Interface-induced superconductivity and strain-dependent spin density wave in FeSe/SrTiO<sub>3</sub> thin films *Nat. Mater.* **12** 634
- [11] Miyata Y, Nakayama K, Sugawara K, Sato T and Takahashi T 2015 High-temperature superconductivity in potassium-coated multilayer FeSe thin films *Nat. Mater.* **14** 775
- [12] Zhang W H *et al* 2014 Interfacial charge doping effect on superconductivity of single unit-cell FeSe films on SrTiO<sub>3</sub> substrates *Phys. Rev. B* **89** 060506(R)
- [13] Bang J *et al* 2013 Atomic and electronic structures of single-layer FeSe on SrTiO<sub>3</sub>(001): the role of oxygen deficiency *Phys. Rev. B* **87** 220503(R)
- [14] Zheng F W, Wang Z G, Kang W and Zhang P 2013 Antiferromagnetic FeSe monolayer on SrTiO<sub>3</sub>: the charge doping and electric field effects *Sci. Rep.* **3** 2213
- [15] Lee J J *et al* 2014 Interfacial mode coupling as the origin of the enhancement of  $T_c$  in FeSe films on SrTiO<sub>3</sub> *Nature* **515** 245
- [16] Choudhury N, Walter E J, Kolesnikov A I and Loong C-K 2008 Large phonon band gap in SrTiO<sub>3</sub> and the vibrational signatures of ferroelectricity in ATiO<sub>3</sub> perovskites: first-principles lattice dynamics and inelastic neutron scattering *Phys. Rev. B* **77** 134111
- [17] Li B, Xing Z W, Huang G Q and Xing D Y 2014 Electron–phonon coupling enhanced by the FeSe/SrTiO<sub>3</sub> interface *J. Appl. Phys.* **115** 193907
- [18] Xie Y, Cao H-Y, Zhou Y, Chen S, Xiang H and Gong X-G 2015 Oxygen vacancy induced flat phonon mode at FeSe/SrTiO<sub>3</sub> interface *Sci. Rep.* **5** 10011
- [19] Tang C J *et al* 2015 Interface enhanced electron–phonon coupling and high temperature superconductivity in potassium-coated ultra-thin FeSe films on SrTiO<sub>3</sub> *Phys. Rev. B* **93** 020507(R)
- [20] Coh S, Cohen M L and Louie S G 2015 Large electron–phonon interactions from FeSe phonons in a monolayer *New J. Phys.* **17** 07302
- [21] Song C-L, Wang Y-L, Jiang Y-P, Li Z, Wang L L, He K, Chen X, Ma X-C and Xue Q-K 2011 Molecular-beam epitaxy and robust superconductivity of stoichiometric FeSe crystalline films on bilayer graphene *Phys. Rev. B* **84** 020503
- [22] Li F S *et al* 2015 Interface-enhanced high-temperature superconductivity in single-unit-cell FeTe<sub>1-x</sub>Se<sub>x</sub> films on SrTiO<sub>3</sub> *Phys. Rev. B* **91** 220503(R)
- [23] Erdman N, Poeppelmeier K R, Asta M, Warschkow O, Ellis D E and Marks L D 2002 The structure and chemistry of the TiO<sub>2</sub>-rich surface of SrTiO<sub>3</sub> (001) *Nature* **419** 55
- [24] Herger R, Willmott P R, Bunk O, Schlepuetz C M, Patterson B D and Delley B 2007 Surface of strontium titanate *Phys. Rev. Lett.* **98** 076102
- [25] Zhu G-Z, Radtke G and Botton G A 2012 Bonding and structure of a reconstructed (001) surface of SrTiO<sub>3</sub> from TEM *Nature* **490** 384
- [26] Kienzle D M, Becerra-Toledo A E and Marks L D 2011 Vacant-site octahedral tilings on SrTiO<sub>3</sub> (001), the ( $\sqrt{13} \times \sqrt{13}$ )R33.7° surface, and related structures *Phys. Rev. Lett.* **106** 176102
- [27] Marshall M S J, Becerra-Toledo A E, Marks L D and Castell M R 2015 *Defects at Oxide Surfaces* (Switzerland: Springer) pp 327–49
- [28] Muller D A, Nakagawa N, Ohtomo A, Grazul J L and Hwang H Y 2004 Atomic-scale imaging of nanoengineered oxygen vacancy profiles in SrTiO<sub>3</sub> *Nature* **430** 657
- [29] Li Z, Peng J-P, Zhang H-M, Song C-L, Ji S-H, Wang L L, He K, Chen X, Xue Q-K and Ma X-C 2015 Visualizing superconductivity in FeSe nanoflakes on SrTiO<sub>3</sub> by scanning tunneling microscopy *Phys. Rev. B* **91** 060509(R)
- [30] Fan Q *et al* 2015 Plain s-wave superconductivity in single-layer FeSe on SrTiO<sub>3</sub> probed by scanning tunnelling microscopy *Nat. Phys.* **11** 946
- [31] Li N, Li Z, Ding H, Ji S H, Chen X and Xue Q-K 2013 An atomic force microscopy study of single-layer FeSe superconductor *Appl. Phys. Express* **6** 113101
- [32] Imai T, Ahilan K, Ning F L, McQueen T M and Cava R J 2009 Why does undoped FeSe become a high- $T_c$  superconductor under pressure? *Phys. Rev. Lett.* **102** 177005
- [33] Moon C-Y and Choi H J 2010 Chalcogen-height dependent magnetic interactions and magnetic order switching in FeSe<sub>x</sub>Te<sub>1-x</sub> *Phys. Rev. Lett.* **104** 057003
- [34] Mizuguchi Y, Hara Y, Deguchi K, Tsuda S, Yamaguchi T, Takeda K, Kotegawa H, Tou H and Takano Y 2010 Anion height dependence of  $T_c$  for the Fe-based superconductor *Supercond. Sci. Technol.* **23** 054013
- [35] Peng R *et al* 2014 Tuning the band structure and superconductivity in single-layer FeSe by interface engineering *Nat. Commun.* **5** 5044
- [36] Zhou G Y *et al* 2015 Observation of interface induced high temperature superconductivity in single unit-cell FeSe films on SrTiO<sub>3</sub>(110) arXiv:1512.01948
- [37] Berlijn T, Cheng H-P, Hirschfeld P J and Ku W 2014 Doping effects of Se vacancies in monolayer FeSe *Phys. Rev. B* **89** 020501
- [38] Shanavas K V and Singh D J 2015 Doping SrTiO<sub>3</sub> supported FeSe by excess atoms and oxygen vacancies *Phys. Rev. B* **92** 035144
- [39] Lee D H 2015 What makes the  $T_c$  of FeSe/SrTiO<sub>3</sub> so high? *Chin. Phys. B* **24** 117405